Spatially Ordered Quantum Dot Array of Indium Nanoclusters in Fully Indium-Exchanged Zeolite X

Nam Ho Heo,* Jong Sam Park, Young Joo Kim, and Woo Taik Lim

Laboratory of Structural Chemistry, Department of Industrial Chemistry, Kyungpook National University, Taegu 702-701, Korea

Sung Wook Jung

Research Institute of Industrial Science and Technology, P. O. Box 135, Pohang 790-600, Korea

Karl Seff*

Department of Chemistry, University of Hawaii at Manoa, Honolulu, Hawaii 96822-2275

Received: August 21, 2002

A spatially ordered quantum dot array of cationic indium nanoclusters has been synthesized in a single crystal of zeolite X. A single crystal of fully dehydrated and fully indium-exchanged zeolite X (ca. $In_{87}Si_{100}Al_{92}O_{384}$, In_{87}−X) was exposed to 0.5 atm of H_2S for 12 h at 673 K. After it was evacuated at temperature and cooled to 294 K, the crystal structure of the product (ca. $In_{66}Si_{100}Al_{92}O_{384}$, In_{66}−X, $a = 24.942(4)$ Å) was determined by single crystal X-ray diffraction techniques in the cubic space group $Fd\bar{3}m$. It was refined with all measured reflections to the final error index $R_1 = 0.058$ for the 754 reflections with $F_o > 4\sigma(F_o)$. X-ray photoelectron spectroscopy experiments confirmed the existence of both atomic and cationic indiums inside the single crystal. The 66 indium atoms or ions per unit cell were found at four crystallographically distinct positions, all on 3-fold axes. Eight In atoms at the sodalite unit centers and 32 $In^{ca.2+}$ ions nearby ($In^{ca.2+}-In^0 = 2.683(1)$ Å), both filling their crystallographic sites, form eight $(In_5)^{n+}$ ($n = 7$ satisfies Lewis's rule) per unit cell, one per sodalite cavity. Each $(In_5)^{n+}$ quantum dot (diameter ca. 7.0 Å) is held in place by 12 strong electrostatic interactions with six ring oxygens ($In^{ca.2+}-O(3) = 2.170(7)$ Å). These quantum dots are arranged in the diamond structure with intercluster distances of ca. 10.8 Å. This crystal (cross-section ca. 0.15 mm) contains ca. 300 Tera (10^{12}) ordered dots of $(In_5)^{n+}$. Another 25 In^+ ions per unit cell were located at a 32-fold site in the supercage, and a single In^{2+} ion was found nearby. Treatment with H_2S has allowed In^+ ions to disproportionate to give full occupancy at the $(In_5)^{n+}$ site.

Introduction

The ability to engineer regular arrangements of identical micro- or nanoparticles of pure substances or composite materials in solid hosts is important in creating for future generations new molecular level electronic, optical, and magnetic devices that are smaller, faster, more selective, and more efficient.[1] Zeolites, with their nanometer-dimensioned window, channel, and cavity architectures, are one of the most promising host materials[2,3] because they require guest units to be both sharply uniform and spatially oriented. The wide range of zeolite frameworks available allows the formation of nanoparticles of various sizes with various orientation patterns.[4,5]

In this regard, various semiconductors, often binary compounds of elements from the main groups III, IV, V, and VI, have been introduced into various zeolites, and their properties, novel due to quantum size effects, have been studied for decades.[1,4−12] For example, clusters of GaP synthesized in the cavities of zeolite Y by chemical vapor deposition techniques were extensively studied.[6,7] InP synthesized in mordenite has shown such an effect with an enhanced energy gap between valence and conduction bands.[8]

ZnS and CdS clusters prepared in zeolite Y show an unusual blue shift in their absorption spectra as compared to the bulk material.[9] The absorption spectra of CdS and PbS clusters synthesized in the cavities of zeolites Y and M, respectively, are greatly shifted to higher energy and have weaker oscillator strengths as compared to the bulk.[9,10] Similarly, Laponite (porous Vycor glass),[11] zeolite X, and sodalite have been used to host small particles of CdS;[12] the optical properties of these materials were studied as a function of Cd^{2+} concentration and were discussed in terms of particle size.[12]

Such chemical species within zeolites may potentially be good catalysts for important reactions. For example, gallium species in ZSM-5 introduced by ion exchange,[13] by impregnation[14] with gallium salts, or by reducing mechanical mixtures of Ga_2O_3 and the zeolite[15,16] were found to be active for the aromatization of light alkanes[13,17] and for hydrocarbon reduction.[18,19] Indium species were also introduced into various zeolites during hydrothermal synthesis[20] or by postsynthesis modification.[21−23] Their catalytic activities were investigated for various reactions such as benzoylation of naphthalene,[20] isomerization of *m*-xylene,[21] and reduction of NO_x with CH_4.[22] That work showed

10.1021/jp0219348 CCC: $25.00
Published on Web 01/08/2003

that In^+ and InO^+ species within the zeolites are at, or closely involved with, the active sites for those reactions.

Numerous attempts to ion exchange In ions into zeolites with high Al content (low Si/Al ratios and therefore high ion exchange capacities), as routes to the formation of group III species in zeolite frameworks, have failed.[4,24] This is due primarily to the loss of zeolite crystallinity that occurs at the low pH values required to keep the group III cations in solution. Other methods involving the use of melts of various anhydrous nitrates and halides have also failed for similar reasons.[4] On the other hand, the physical inclusion of indium metal into the lattice of zeolite A was reported by Alekseev et al. at extreme conditions, such as 20 kbar of pressure.[25,26] Just from a consideration of the unit cell formula, $Na_{12}-A(8In)$ and the geometry of the zeolite, they proposed some possible structures.[25,26]

Attempts to introduce In species into zeolites with relatively high Si content (low ion exchange capacities) by ion-exchange and subsequent reaction have also been reported. Uchida et al., by aqueous ion exchange of In^{3+} into mordenite (Si/Al ratio ca. 9.6), achieved nearly 71% exchange (ca. 11.3 wt % indium).[12] Kanazirev et al. have reported the inclusion of relatively small amounts of In species (ca. 3.66 wt % as oxide), probably In^+ as claimed, in zeolite ZSM-5 (Si/Al ratio of the synthesis gel ca. 3.5) by mixing In_2O_3 and the zeolite, followed by reduction with hydrogen.[16,23]

Recently, high concentrations (ca. 44 wt %) of indium species were introduced into zeolites with high Al content (zeolite A with Si/Al probably ca. 1.0, although reported to be a bit greater, ca. 1.04,[27] and zeolite X[28] with Si/Al ca. 1.09). This was accomplished by using solvent-free redox reactions[29−31] between Tl^+ ions and In metal in the zeolites.[32−35] The expected redox reaction ($Tl^+ + In^0 \rightarrow In^+ + Tl^0$) occurred within the zeolites to produce indium zeolites (In−A and In−X) free of Tl. However, the In^+ ions in the products had further disproportionated[36] ($2In^+ \rightarrow In^{2+} + In^0$ or $3In^+ \rightarrow In^{3+} + 2In^0$) to give In in a mixture of oxidation states (In^0, In^+, In^{2+}, and In^{3+}) and with various degrees of clustering.[37,38] Minor changes in the occupancies and distributions of various indium species occurred upon exposure to the atmosphere or to sorbates such as H_2O, H_2S, or sulfur, due to additional disproprotionation.[32−35] The In^0 atoms might have remained inside the zeolite during the redox reaction as left over reactant or, more reasonably, might have formed by disproportionation. They are well-stabilized by forming, with cationic indium species in the zeolite cavities, nanosized clusters such as $(In_3)^{2+}$ and $(In_5)^{n+}$ ($n = 7$ satisfies Lewis's rule).

The nanosized $(In_5)^{n+}$ clusters were repeatedly identified in many crystal structures of In−A and In−X and of their sorption complexes with S and H_2S with various occupancies, all less than full and therefore forming incomplete arrays.[32−35] About 50% of the sodalite units contained $(In_5)^{n+}$ when In−A was prepared by solvent-free redox methods.[32] Upon exposure to H_2S, this value rose to 60%.[35] It increased to almost 75% when it was exposed to sulfur.[33] In zeolite X, about 25% of sodalite units were occupied with $(In_5)^{n+}$ when it was prepared, and washing and redehydration caused a small increase to 31%.[34] These partial occupancies indicate incomplete arrays of $(In_5)^{n+}$ clusters.

In this work, completely indium-exchanged zeolite X (ca. $In_{87}Si_{100}Al_{92}O_{384}$, $In_{87}-X$),[34] prepared by solvent-free redox reaction between In^0 and Tl^+ ions within Tl−X ($Tl_{92}Si_{100}Al_{92}O_{384}$) followed by washing and redehydration, was exposed to H_2S with the hope that further disproprotionation would produce more In^0 atoms and $In^{ca.2+}$ ions and therefore more $(In_5)^{n+}$ inside the zeolite structure. We hoped eventually to achieve full occupancy in the sodalite units, creating a complete three-dimensional quantum dot array of $(In_5)^{n+}$ clusters throughout the resulting single crystal. Zeolites with complete three-dimensional quantum dot arrays of indium clusters might be immediately useful as optical and electronic materials or as catalysts or may be precursors in the preparation of such materials.

Experimental Section

Large single crystals of sodium zeolite X, stoichiometry $Na_{92}Si_{100}Al_{92}O_{384}$ per unit cell ($Na_{92}-X$, Na−X), were prepared in St. Petersburg, Russia.[28] Colorless single crystals, octahedra about 0.15 mm in cross-section, were lodged in a fine Pyrex capillary. Fully Tl^+-exchanged zeolite X ($Tl_{92}Si_{100}Al_{92}O_{384}$, $Tl_{92}-X$, Tl−X) was prepared by the flow method, the dynamic ion exchange of these crystals with 0.1 M aqueous thallous acetate (pH = 6.4, Aldrich Chemical Co., 99.99%).[34,39−41] This and similar ion exchanges had been shown to be suitable for the preparation of stoichiometric Tl−X.[34,39−41]

Several crystals of colorless Tl−X were completely dehydrated (623 K and 1×10^{-6} Torr for 48 h)[34,39−41] and were brought into contact with In^0 (Aldrich Chemical Co., 99.999%) in fine Pyrex capillaries at 623 K for 96 h. This was achieved under vacuum as described and discussed before,[32−35] by condensing In^0 around the crystals whose temperature was somewhat lower than that of the metal in coaxially connected cylindrical ovens. Although the vapor pressure of In(l) is reported to be very low at 623 K (ca. 2.92×10^{-10} N/m^2 = 2.19×10^{-12} Torr),[42] droplets of In were seen to form very close to the zeolite crystals. At 623 K, the vapor pressure of Tl(s) is 1.22×10^{-6} Torr (1.63×10^{-4} N/m^2);[42] any elemental thallium produced could readily distill away from the crystal. Other experimental procedures for the reaction and characterization of products were similar in detail to those previously described for the preparations of In−A[32,33,35] and $In_{87}-X$.[34]

One of the resulting black crystals, still under vacuum in its capillary, was then exposed to the atmosphere and was washed with deionized water, hoping to remove any residual Tl or In species that might be present on the surface of the crystal, as was done in the preparations of In−A, $In_{88}-X$, and $In_{87}-X$.[32−35] This crystal, still black after washing, was lodged in a fine Pyrex capillary and then dehydrated at 623 K and 1×10^{-6} Torr for 48 h. Finally, the redehydrated crystal (still black) was exposed to 0.5 atm of zeolitically dried H_2S (Aldrich Chemical Co., 99.999%) for 12 h at 673 K. After it was evacuated at temperature, the crystal was sealed off from the vacuum line at room temperature for X-ray experiments, followed by electron probe microanalysis and x-ray photoelectron spectroscopy (XPS) experiments. The crystal had a metallic gray powder on its surface; just from its appearance, this powder may be one or more of the following: In_2O, In_2S, InS, and finely divided In. In_2S and InS seem most likely because In_2O and In are more volatile and should have distilled away.[32−35]

Electron probe X-ray microanalysis (EPXMA) of the product single crystal after exposure to the atmosphere was carried out with a EDAX 9100 system, an energy dispersive spectrometer (EDS) system attached to a Phillips 515 SEM. XPS experiments for the product single crystal were also performed by using a VG ESCALAB 250 instrument with Al Kα (1486.7 eV) radiation for excitation at 15 KV and 10 mA and an ion gun at 3.0 KV for sputtering (0.6 Å/s) to obtain depth profiles. The resulting EDS and XPS (for In 3d electrons) spectra are shown

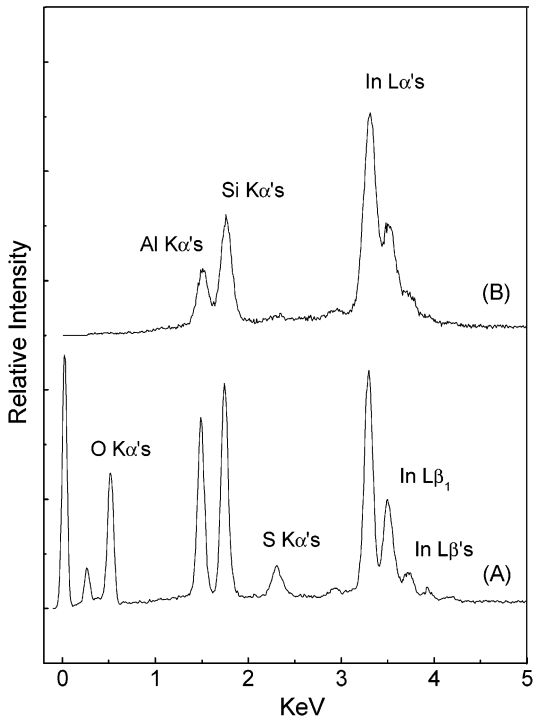

Figure 1. EPXMA spectra of the product $In_{66}-X$ (A) and the reactant $In_{87}-X$ (B) single crystals. (Spectrum B was copied from ref 34).

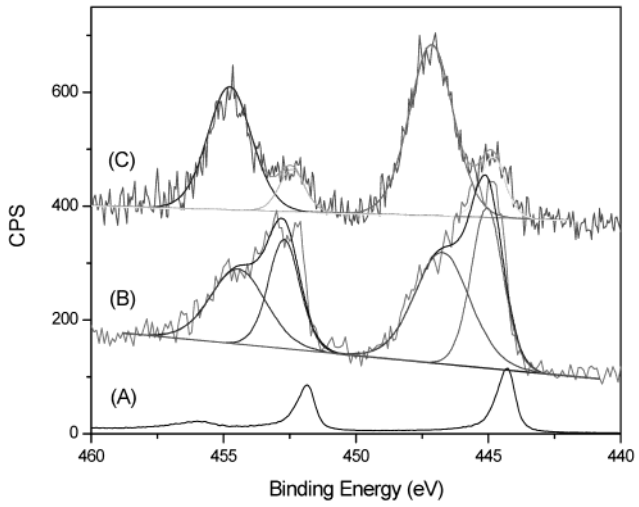

Figure 2. XPS spectra of the In 3d electrons in In metal (A) and in single crystals of $In_{66}-X$ (B) and $In_{87}-X$ (C). The intensities in the spectrum of In metal were reduced by 1/20 for clear comparison.

in Figures 1 and 2, respectively, each with the corresponding spectrum of a reactant $In_{87}-X$ single crystal. The XPS depth profiles of the In 3d electrons in the product are presented in Figure 3.

X-ray Data Collection. The space groups $Fd\bar{3}$ and $Fd\bar{3}m$,[34,43] which are consistent with the reflection conditions (*hkl*: $h + k$, $k + l$, $l + h = 2n$; 0*kl*: $k + l = 4n$), were both carefully considered. However, the space group $Fd\bar{3}m$ was eventually selected because of the intensity equality observed for *hkl* and *khl* reflections and because of the refinement results in $Fd\bar{3}$: the Si−O and Al−O distances, by being nearly the same, indicated that long-range Si/Al ordering had essentially been lost.[44,45] Also, the error indices after least-squares refinement were lower in $Fd\bar{3}m$. Details of the crystallographic refinement carried out in both space groups are summarized in Table 1.

A CAD4/Turbo diffractometer equipped with a rotating anode generator and a graphite monochromator was used for preliminary experiments and for the subsequent collection of diffraction intensities, all at 294 K using molybdenum radiation. The unit cell constant, $a = 24.942(4)$ Å, was determined by a least-squares treatment of 25 intense reflections in diverse regions of reciprocal space. Background intensity was counted at each end of a scan range for a time equal to half the scan time. The intensities of three reflections in diverse regions were recorded every 3 h to monitor crystal and instrumental stability. Only small random fluctuations of these check reflections were observed during the course of data collection. The number of 4σ intensities is remarkably large (see Table 1), indicating that this crystal has good crystallinity, and suggesting that it contains well-ordered (strongly scattering) substructures. Finally, an absorption correction ($\mu = 2.20$ mm^{-1})[46] was made using the semiempirical ψ-scan method. The corrected data gave nearly the same final *R* values, so the correction was not used. Other experimental details as well as a summary of the crystallographic data are given in Table 1.

Structure Determination. Full-matrix least-squares refinements (SHELXL97)[47] were done on F^2 using all reflections without an $n\sigma$ cutoff. They were initiated with the atomic positions of the framework atoms [(Si,Al), O(1), O(2), O(3), and O(4)] and the major In position from previously reported structures of dehydrated $In_{87}-X$[34] [In^+ at In(II)]. A refinement with anisotropic thermal parameters for all framework atoms in this model, with In(II) refining isotropically, converged to the error index $R_1 = 0.48$ with an occupancy of 24.3(2) at In(II). Introducing In(U) as In^0 atoms at a peak (0.125,0.125,0.125) from a difference Fourier function reduced R_1 to 0.46 with resulting occupancies of 22.8(2) and 4.6(5) at In(II) and In(U), respectively. Adding In(I′) isotropically as In^{2+} at another peak (0.063,0.063,0.063) found in a subsequent difference function converged with R_1 sharply reduced to 0.063 with resulting occupancies of 25.9(4), 8.0(1), and 32.4(4) at In(II), In(U), and In(I′), respectively. Including In(IIa) isotropically as In^{2+} at a peak (0.23,0.23,0.23) found in a difference function based on this model converged and further reduced R_1 to 0.062 with occupancies of 25.0(4), 7.9(1), 31.7(3), and 0.8(2) at In(II), In(U), In(I′), and In(IIa), respectively. All In positions were refined anisotropically in the final cycles of refinement with occupancies fixed at 25, 8, 32, and 1 at In(II), In(U), In(I′), and In(IIa), respectively. This converged to the final error index $R_1 = 0.058$. The difference Fourier function based on this model was featureless except for some peaks opposite a four ring in the supercage. Efforts to introduce those peaks as In or S species were unsuccessful; they were always unstable in refinement. The final structural parameters are presented in Table 2, and selected interatomic distances and angles are in Table 3.

Fixed weights were used initially; the final weights were assigned using the formula $w = 1/[\sigma^2(F_o^2) + (aP)^2 + bP]$ where $P = [\max(F_o^2,0) + 2F_c^2]/3$, with $a = 0.0789$ and $b = 296.55$ as refined parameters (see Table 1). Atomic scattering factors for In, In^+, In^{2+}, O^-, and $(Si,Al)^{1.75+}$ were used.[48,49] Oxidation states were assigned to the indium positions according to their distances to framework oxygens (vide infra). Scattering factors of In^{2+} and In^+ were calculated from those of In^{3+} and In^0 as follows: $(2In^{3+} + In^0)/3$ and $(In^{3+} + 2In^0)/3$, respectively. The function describing $(Si,Al)^{1.75+}$ is the mean of the Si^{4+}, Si^0, Al^{3+}, and Al^0 functions. All scattering factors were modified to account for anomalous dispersion.[50,51]

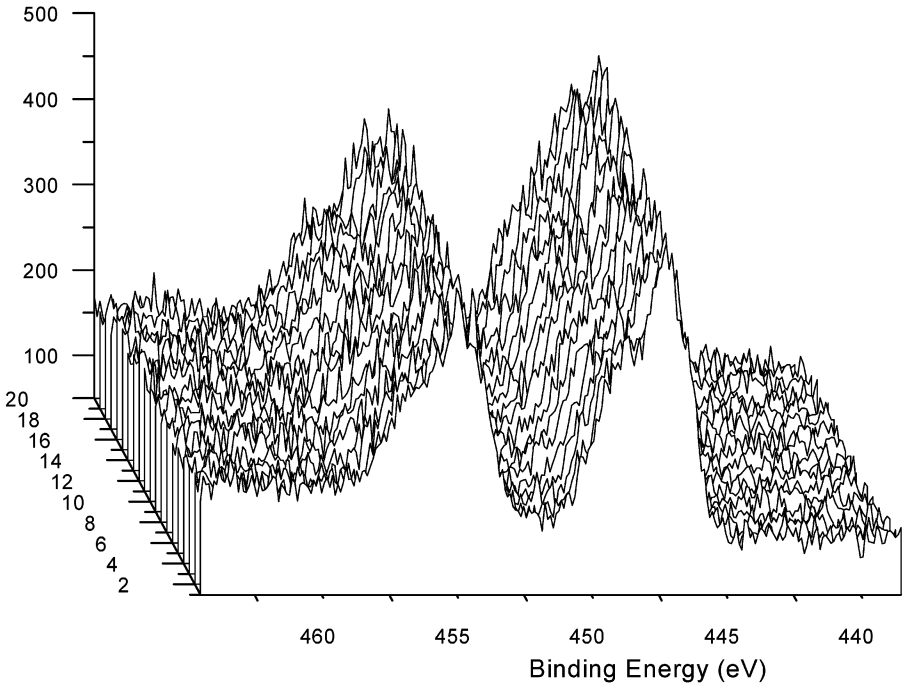

Figure 3. Depth profile for the In 3d electrons in the $In_{66}-X$ single crystal after consecutive sputtering treatments. Sputtering (0.6 Å/s) was done for about 10 s after each measurement.

TABLE 1: Summary of Experimental and Crystallographic Data

cryst cross-section (mm)	0.15	
ion exchange for Tl^+ (days/mL/K)	4/10.0/298	
dehydration of Tl−X (days/K)	3/673	
reaction of Tl−X with In (days/K)	5/623	
washing of In−X with DI water (days/mL)	1/10.0	
redehydration of In−X (days/K)	3/673	
exposure to H_2S (atm/h/K)	0.5/12/673	
evacuation (min/K)	10.0/673	
temp for data collection (K)	294	
X-radiation (Mo Kα) λ_1/λ_2 (Å)	0.70930/0.71359	
unit cell constant, a_0 (Å)	24.942(4)	
no. of reflections for a_0	25	
scan technique	$\omega-2\theta$	
scan speed (deg 2θ/min)	0.5	
scan width (deg)	$0.51 + 0.61*\tan\theta$	
2θ range for a_0 (deg)	10−20	
2θ range in data collection (deg)	2−70	
space group/no.	$Fd\bar{3}m$/227	$Fd\bar{3}$/203
no. of reflections measured	2335	2335
no. of unique reflections, m	1209	2032
no. of reflections ($F_o > 4\sigma(F_o)$)	754	1207
no. of parameters, s	44	66
data/parameter ratio, m/s	17.1	18.3
weighting parameters, a/b	0.0789/296.55	0.0677/620.90
R_1 ($F_o > 4\sigma(F_o)$)[a]	0.0583	0.0691
wR_2 (all unique data)[b]	0.183	0.187
goodness of fit[c]	1.112	1.080

[a] $R_1 = \Sigma(|F_o - |F_c||)/\Sigma F_o$. [b] $wR_2 = [\Sigma\{w(F_o^2 - F_c^2)^2\}/\Sigma w(F_o^2)^2]^{1/2}$. [c] $[\Sigma\{w(F_o^2 - F_c^2)^2\}/(m - s)]^{1/2}$, where m and s are the numbers of unique reflections and parameters, respectively.

Results and Discussion

EPXMA. The EDS spectrum of the final product (A) in Figure 1 shows several peaks corresponding to O ($K\alpha_{1,2}$, $K\alpha_1$, and $K\alpha_2$ are at 0.53, 0.53, and 0.52 keV, respectively), Al ($K\alpha_1$, $K\alpha_2$, and $K\alpha_{1,2}$ overlap at 1.49 keV), and Si ($K\alpha_1$, $K\alpha_{1,2}$, and $K\alpha_2$ overlap at 1.74 keV) of the zeolite framework.[52] The Kα lines of Al and Si appear consistently in both the reactant and the product crystals with almost the same relative intensities, indicating that the composition of the zeolite framework was not significantly altered by the sorption experiment.[34] The absence of peaks corresponding to O in spectrum B is probably due to the window material (Be) used previously.[34] The strong Lα and Lβ lines of In ($L\alpha_1$ at 3.28 keV and $L\alpha_2$ at 3.29 keV; $L\beta_1$, $L\beta_2$, and $L\beta_3$ at 3.49, 3.71, and 3.57 keV, respectively) are nearly the same in the product (spectrum A) and in the reactant (spectrum B) crystals. The absence of Tl lines ($M\alpha_1$ and $M\alpha_2$ lines overlapping at 2.27 keV) indicate again in spectrum A that the replacement of Tl^+ by In species is complete (as had been seen in spectrum B), confirming that fully indium-exchanged zeolite X ($In_{87}-X$) free of Tl had been successfully prepared.[34,52] Further EPXMA experiments using the fresh surface of an intentionally broken reactant crystal ($In_{87}-X$) also confirmed that In is the only nonframework element present.

Spectrum A also shows that the final product is an indium aluminosilicate containing sulfur (in some chemical form), probably on the surface because EPXMA is a surface sensitive technique and because sulfur atoms are not seen in the crystal structure of the final product ($In_{66}-X$, vide infra). The strong $K\alpha_{1,2}$ and $K\alpha_2$ lines of S (overlapping at 2.31 keV) might have been assigned as Mα lines of Tl (2.27 keV, vide supra), but the absence of additional strong $L\alpha_1$ and $L\beta_1$ lines at 10.26 and 12.21 keV, respectively, for Tl and the presence of a peak at ca. 0.10 keV, which may contain the strong L_l and L_n lines of S (both at 0.15 keV), confirm this assignment. The peak observed at ca. 0.30 keV in spectrum A corresponds to the common Kα lines of C (0.28 keV) from contamination by carbonaceous materials, while the peak at ca. 0.10 keV is a frequent ghost for the instrument used.

XPS Analyses. The XPS experiments showed that both the reactant and the product In−X crystals contain indium in various oxidation states as shown in Figure 2. First of all, the XPS spectrum of indium metal (A) shows two strong indium photoelectron peaks corresponding to $3d_{3/2}$ and $3d_{5/2}$ electrons (at ca. 451.8 and 444.3 eV, respectively; ΔE = ca. 7.5 eV). A weak ghost peak is seen at a higher binding energy.

TABLE 2: Positional, Thermal, and Occupancy Parameters[a] of $In_{66}-X$

	Wyckoff position	*x*	*y*	*z*	U_{11}	U_{22}	U_{33}	U_{12}	U_{13}	U_{23}	occupancy fixed	occupancy varied
(Si,Al)	192(*i*)	−5168(8)	12 413(8)	3640(7)	108(9)	68(8)	90(9)	−23(7)	−11(6)	−1(7)	192[c]	
O(1)	96(*h*)	−10 116(20)	0[d]	10 116(20)	210(24)	184(39)	210(24)	−71(21)	31(29)	−71(21)	96	
O(2)	96(*g*)	26(24)	26(24)	14 727(29)	193(22)	193(22)	189(39)	6(22)	6(22)	56(31)	96	
O(3)	96(*g*)	−2337(28)	7097(19)	7097(19)	122(34)	143(21)	143(21)	−3(25)	27(18)	27(18)	96	
O(4)	96(*g*)	7826(22)	7826(22)	31 976(29)	197(24)	197(24)	154(39)	40(20)	40(20)	50(28)	96	
In(U)	8(*a*)	12 500[d]	12 500[d]	12 500[d]	146(5)	146(5)	146(5)	0	0	0	8	7.9(1)
In(I′)	32(*e*)	6289(3)	6289(3)	6289(3)	159(3)	159(3)	159(3)	−18(3)	−18(3)	−18(3)	32	31.7(3)
In(II)	32(*e*)	25 149(5)	25 149(5)	25 149(5)	271(5)	271(5)	271(5)	−23(6)	−23(6)	−23(6)	25	25.0(4)
In(IIa)	32(*e*)	23 480(194)	23 480(194)	23 480(194)	295(137)	295(137)	295(137)	229(178)	229(178)	229(178)	1	0.8(2)

[a] Positional parameters are given × 10^5; thermal parameters are given × 10^4. Numbers in parentheses are the estimated standard deviations in the units of the least significant figure given for the corresponding parameter. The anisotropic temperature factor is $\exp[-2\pi^2a^{-2}(U_{11}h^2 + U_{22}k^2 + U_{33}l^2 + 2U_{12}hk + 2U_{13}hl + 2U_{23}kl)]$. [b] Occupancy factors are given as the number of atoms or ions per unit cell. [c] Occupancy for (Si) = 96 and (Al) = 96. [d] Fixed by symmetry.

TABLE 3: Selected Interatomic Distances (Å) and Angles (deg)[a]

(Si,Al)−O(1)	1.636(3)	O(1)−(Si,Al)−O(2)	113.9(3)
(Si,Al)−O(2)	1.681(4)	O(1)−(Si,Al)−O(3)	108.4(3)
(Si,Al)−O(3)	1.732(4)	O(1)−(Si,Al)−O(4)	113.5(4)
(Si,Al)−O(4)	1.644(3)	O(2)−(Si,Al)−O(3)	102.5(3)
mean of (Si,Al)−O	1.673(4)	O(2)−(Si,Al)−O(4)	107.8(4)
		O(3)−(Si,Al)−O(4)	110.5(4)
In(I′)−O(3)	2.170(7)		
In(II)−O(2)	2.600(7)	In(U)−In(I′)	2.6831(13)
In(IIa)−O(2)	2.246(32)		
		In(I′)−In(U)−In(I′)	109.47[b]
(Si,Al)−O(1)−(Si,Al)	146.8(5)	O(2)−In(II)−O(2)	88.1(3)
(Si,Al)−O(2)−(Si,Al)	135.2(5)	O(2)−In(IIa)−O(2)	111.7(20)
(Si,Al)−O(3)−(Si,Al)	126.6(4)	O(3)−In(I′)−O(3)	100.10 (23)
(Si,Al)−O(4)−(Si,Al)	147.4(5)		

[a] Numbers in parentheses are the estimated standard deviations in the units of the least significant digit given for the corresponding parameter. [b] Exactly the tetrahedral angle by symmetry.

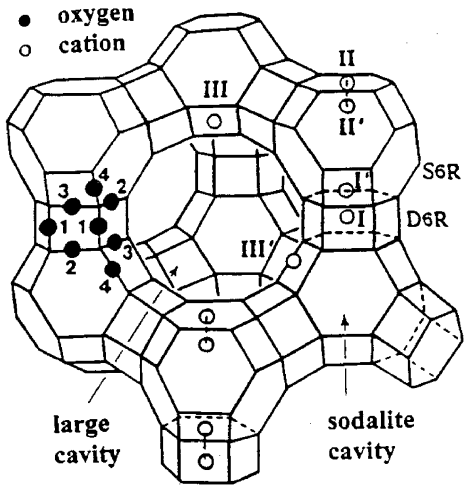

Figure 4. Stylized drawing of the framework structure of zeolite X. Near the center of the each line segment is an oxygen atom. The different oxygen atoms are indicated by the numbers 1−4. Silicon and aluminum atoms alternate at the tetrahedral intersections, except that Si substitutes for Al at about 4% of the Al positions. Extra framework cation positions are labeled with Roman numerals. Site U is at the center of the sodalite cavity.

In spectrum B ($In_{66}-X$) and spectrum C ($In_{87}-X$), at least two pairs of peaks ($3d_{3/2}$ and $3d_{5/2}$ with similar relative intensities) were observed for the binding energies of the indium d electrons. The pair with the smaller binding energies (at ca. 452.5 and 445.0 eV for the $3d_{3/2}$ and $3d_{5/2}$ electrons, respectively, ΔE = ca. 7.5 eV also) matches those of the 3d electrons of In^0 in indium metal (vide supra) relatively well;[53] the slightly higher binding energies (ca. 0.7 eV) of the In^0 3d electrons in In−X can be considered evidence of their interaction with indium cations. The second pair of peaks has substantially higher binding energies (ca. 454.7 and 447.2 eV for the corresponding 3d electrons, again with ΔE = ca. 7.5 eV). This suggests that oxidation states higher than 0 must exist in all In−X crystals. Considering the available binding energies of the $3d_{5/2}$ electrons in bulk InCl (in the range of ca. 444.6−445.2 eV), $InCl_3$ (ca. 446.0−446.9 eV), and other compounds of In^{3+} with less electrophilic anions (444.1−446.3 eV),[53] the oxidation states of the indium cations in In−X (binding energy of ca.. 447.2 eV for $3d_{5/2}$ electrons) must be between 1+ and 3+.

Furthermore, and more importantly, the intensities of the lower energy pair of peaks in spectrum B, those of the indium atoms, are much greater than those in spectrum C, indicating that more indium atoms are present in the final product, even though $In_{66}-X$ contains fewer indium atoms and ions than $In_{87}-X$. Because XPS is also a surface sensitive technique, similar experiments were conducted to examine the depth profile of indium species after consecutive sputtering with argon.[54] As shown in Figure 3, the depth profile spectra confirm the presence of indium in various oxidation states, in atomic and higher oxidation states, inside the product In−X single crystal, down to a depth of ca. 4300 Å. This and the crystal structure (vide infra) confirm that indium atoms and cations are simultaneously present throughout the body of the In−X single crystal.

General Description of Zeolite X. Zeolite X is a synthetic Al-rich analogue of the naturally occurring mineral faujasite. The 14-hedron with 24 vertexes known as the sodalite cavity or β-cage may be viewed as the principal building block of the aluminosilicate framework of the zeolite (see Figure 4). These sodalite units are connected tetrahedrally at six rings by bridging oxygens to give double six rings (D6Rs, hexagonal prisms) and, concomitantly, to give an interconnected set of even larger cavities (supercages) accessible in three dimensions through 12 ring (24-membered) windows. The Si and Al atoms occupy the vertexes of these polyhedra. The oxygen atoms lie approximately halfway between each pair of Si and Al atoms but are displaced from those points to give near tetrahedral angles about Si and Al.

Exchangeable cations that balance the negative charge of the aluminosilicate framework are found within the zeolite's cavities. They are usually found at the following sites shown in Figure 4: site I at the center of a D6R, I′ in the sodalite cavity on the opposite side of either of the D6R's six rings from site I, II′ inside the sodalite cavity near a single six ring (S6R) entrance to the supercage, II opposite a S6R in the supercage, III on a 2-fold axis opposite an O(3)−O(4)−O(3)−O(4) four ring (between two 12 rings) in the supercage, and III′ somewhat

or substantially off the 2-fold axis but otherwise on the inner surface of the supercage or near a 12 ring.[55,56]

Space Group Considerations. If the Si and Al atoms alternate in the zeolite X framework in obeyance of Loewenstein's rule,[57] then the space group of zeolite X is $Fd\bar{3}$. This is true even though about 4% of the Al sites are occupied by Si atoms to accommodate the excess Si atoms in $Na_{92}Si_{100}Al_{92}O_{384}$.[28] This ordering of Si and Al atoms is confirmed by the average values of the Si−O (1.62 Å) and Al−O (1.72 Å) distances that are commonly seen. However, the In_{66}−X data were refined using the space group $Fd\bar{3}m$ due to the mirror planes observed in reciprocal space at (110); the experimentally observed intensity equality between *hkl* and *khl* pairs of reflections indicate that the Si and Al atoms are no longer ordered in the framework structure of In_{66}−X. Furthermore, when it was refined using $Fd\bar{3}$, the averaged "Si"−O and "Al"−O distances, 1.66 and 1.68 Å, respectively, are essentially the same, not allowing the conclusion that one position (in $Fd\bar{3}$) is richer in either Si or Al than the other. The long-range Si/Al ordering presumed to be uniformly present in the batch supply[28] of Na_{92}−X[58] used and initially present in Tl_{92}−X[39−41] and unwashed In_{88}−X[34] has therefore been lost.[43,44,58−61]

Crystal Structure of In_{66}−X. The structural parameters of the framework atoms in In_{66}−X are very similar to those previously reported for In_{88}−X and In_{87}−X.[34] The indium positions have also been seen before. However, in addition to the sharp decrease in the number of In atoms and ions per unit cell, the number of indium positions in In_{66}−X and their occupancies are very different from those found in In_{88}−X and In_{87}−X. There are only four indium positions in In_{66}−X.

(a) Assignment of Tentative Oxidation States. The oxidation state (best integer) at each indium position is identified on the basis of its approach distance to framework atoms and to each other, with the general expectation that indium ions nearest to framework oxygens should have the highest cationic charges. This reasoning is frequently used, e.g., with In−A,[32] In−A(S_2),[33] In_{88}−X, and In_{87}−X.[34] In addition, the final assignment must give a structure that is electrically neutral, although allowance may be made for undetectable H^+ ions or framework oxygens that may be missing.

With 66 In atoms or ions whose charges need to sum to 92+ per unit cell and the evidence from the XPS spectra of In_{66}−X for the presence of various oxidation states, it is clear that a mix of oxidation states is present. In each unit cell of In_{66}−X, the 66 indium atoms or ions occupy four crystallographically distinct positions, all on 3-fold axes, three highly populated (sites U, I′, and II). Among those, eight In^0 atoms fully occupy site U (an In^0 atom is at the center of each sodalite unit) and 32 In^{2+} ions fully occupy site I′ (four In^{2+} ions are opposite D6Rs in each sodalite unit). Opposite S6Rs, 25 In^+ ions per unit cell mostly fill the 32-fold site II. Finally, one In^{2+} ion per unit cell was found at another site II, somewhat closer to the plane of its S6R. These assignments of oxidation state are justified in detail in the following sections. (In the next paragraph, the charge at In(I′) is modified in a small way.)

By the above assignment of oxidation states, the In^0 atom (at site U) and the four In^{2+} ions (at site I′) arranged tetrahedrally about it in each sodalite unit form an $(In_5)^{8+}$ cation. $(In_5)^{8+}$ is an odd electron species with only seven electrons about the central atom, in violation of G. N. Lewis's octet rule. It is unlikely to exist, especially at the high occupancy observed, and is unlikely to have survived the high synthesis temperature. In addition, this centered tetrahedral In cluster is ubiquitous in In zeolites: it was seen in In−A,[32] In−A(S_2),[33] In−A(xInSH),[35] In_{88}−X, and In_{87}−X;[34] the In(I′)/In(U) ratio has consistently been 4.0. $(In_5)^{7+}$, however, is even, satisfies Lewis's octet rule, and is consistent with the crystallographic results (which cannot distinguish between $In^{1.75+}$−O and In^{2+}−O on the basis of bond lengths). Without resolving this issue at this point (additional physical evidence and reasoning is presented in the following several sections), but choosing the more likely result and for simplicity, $In^{ca.2+}$ or $In^{1.75+}$ for the In ion at site I′ and $(In_5)^{n+}$ or $(In_5)^{7+}$ for the nanoclusters in the sodalite units will be used throughout the remainder of this paper.

TABLE 4: Deviations of Guest Ions and Atoms (Å) from (111) Planes of Six Rings

ions or atoms	site	charge	deviation	ions or atoms	site	charge	deviation
At O(2)s of S6Rs[a]				At O(3)s of D6Rs[b]			
In(II)	II	1+	1.55	In(I′)	I′	ca. 2+	1.01
In(IIa)	II	2+	0.83	In(U)[c]	U	0	3.69

[a] A positive deviation indicates that the ion lies in the supercage. [b] A positive deviation indicates that the ion or atom lies in the sodalite unit. [c] At the very center of the sodalite unit.

TABLE 5: Radii[a] (Å) of Indium Ions in Fully Indium-Exchanged Zeolites

	oxidation no. and sites (zeolites A/X)			
	1+			1.75+ or 2+
crystal	I′[b]/II[c]	I′[d]/I′[d]	II[e,f]/III′[f,g]	I′[d]/ I′[d]
In−A[h]	1.253	1.341	1.290	1.039
In−A(S_2)[i]	1.258	1.19	1.29	1.046
In−A(H_2S)[j]	1.255	1.367	1.29	1.032
average	1.255	1.30	1.29	1.039
In_{88}−X[k,l]	1.254	1.206	1.20	0.933
In_{87}−X[k,m]	1.290	1.188	1.31	0.908
average	1.272	1.197	1.26	0.921
In_{66}−X[l]	1.281			0.852
In_{66}−X[m]	1.280			0.850
average	1.281			0.851

[a] The radius was calculated by subtracting that of O^- (1.320 Å) from its approach distance to the nearest framework oxygen. [b] Opposite six ring in the large cavity. [c] Opposite six ring in the supercage. [d] Opposite six ring in the sodalite unit. [e] Near the eight ring in the large cavity. [f] Averaged when more than one position is present at this site. [g] Opposite four rings in the supercage. [h] Data from ref 32. [i] Data from ref 33. [j] Data from ref 35. [k] Data from ref 34. [l] Refined in the space group $Fd\bar{3}$. [m] Refined in the space group $Fd\bar{3}m$.

The In^+ ions found in In_{66}−X are apparently the product of the redox reaction $Tl^+ + In^0 \rightarrow In^+ + Tl^0$. The In^{2+} or $In^{ca.2+}$ ions could have formed similarly or may be viewed as a product of the disproportionation of In^+, e.g., $2In^+ \rightarrow In^{2+} + In^0$, during the high-temperature H_2S treatment. Even the $(In_5)^{7+}$ cluster may have formed by a similar reaction, $7\ In^+ \rightarrow (In_5)^{7+} + 2\ In^0$. As a result of such disproportionation reactions, there are more $In^{ca.2+}$ ions (33) than In^+ ions (25) in In_{66}−X although most indiums are In^+ in In_{88}−X and In_{87}−X. This has presumably occurred because of the great stability of $(In_5)^{7+}$ within the zeolite. It should be noted that the initially greater number of In^+ ions was better able to locally balance the negative charges of the framework oxygens by being able to approach more of them. Because of this, the zeolite framework should have inhibited the formation of In in oxidation states greater than 1+.

(b) Monopositive Indium Ions at Site II. The 25 ions per unit cell at In(II) almost fill this 32-fold site. Each of these ions lies relatively far inside the supercage, 1.55 Å from the (111) plane of three O(2) framework oxygens of the S6R to which it is bound (see Table 4). They are 2.600(7) Å from these O(2)

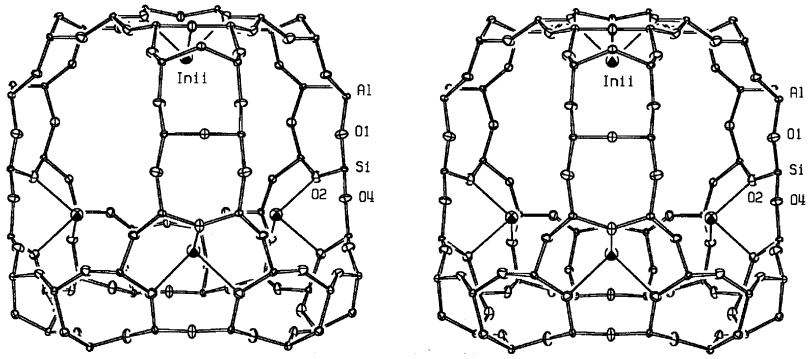

Figure 5. Stereoview of a supercage in $In_{66}-X$. Four In^+ ions are tetrahedrally arranged at In(II). Most supercages (ca. 87.5%) have three such In^+ at In(II) with In at In(IIa) in one of them. The zeolite framework is drawn with thicker bonds. The coordination about In^+ cations is indicated by finer lines. Ellipsoids of 50% probability are shown.

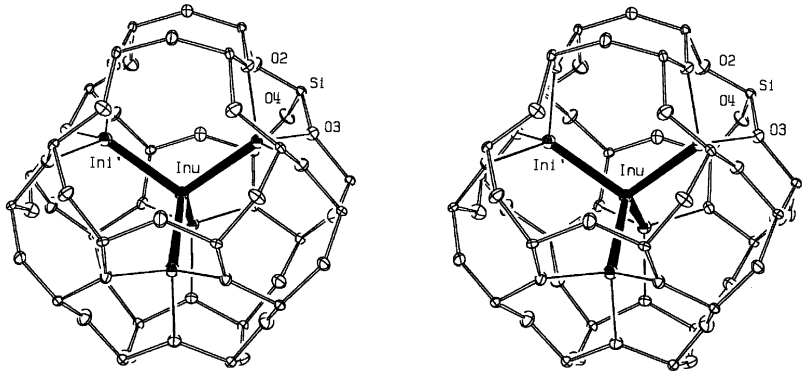

Figure 6. Stereoview of a sodalite unit in $In_{66}-X$ with an In_5^{n+} cluster in its center. In_5^{n+}, shown with solid bonds, is viewed as an In atom at In(U) surrounded by four tetrahedrally arranged $In^{ca.2+}$ ions at In(I′). Each ion at In(I′) coordinates further to three D6R oxygens at O(3). All sodalite units of the $In_{66}-X$ single crystal have such In_5^{n+} clusters in them; $n = 7$ is proposed. See the caption to Figure 5 for other details.

oxygens (see Table 3). Considering the ionic radii of the framework oxygens to be 1.32 Å,[62,63] the radii of these indium ions must be ca. 2.60−1.32 = 1.28 Å, almost identical to those, 1.25, 1.25, and 1.29 Å, found for In^+ ions in $In_{11}-A$, $In_{88}-X$, and $In_{87}-X$, respectively (see Table 5).[32,34] This is somewhat shorter than those found for In^+ in various indium halides, which range from 1.32 to 1.51 Å.[64−66] However, similarly shortened radii have been found for Tl^+ ions in zeolites; ca. 1.30 vs ca. 1.47 Å in various thallium halides, respectively,[32,39−41,67] probably due to the low coordination number of these ions in the dehydrated zeolites. An even smaller radius, 1.17 Å, was suggested for In^+ by a theoretical calculation using the numerical HF method.[68] Accordingly, considering also the arguments in the previous reports of the structures of In−A and In−X and the high occupancy at In(II), the oxidation state of the cations at In(II) appears to be 1+. Some supercages would have four tetrahedrally arranged In^+ ions at In(II), opposite S6Rs, but most will have just three In^+ ions at these sites. A stereoview of the tetrahedral arrangement in a supercage of $In_{66}-X$ is shown in Figure 5.

(c) Dipositive Indium Ions at Sites I′ (more likely 1.75+) and II′. In cations at In(I′) completely fill the 32-fold site I′ (Table 2). Each cation at In(I′) is 2.170(7) Å from three six ring oxygens at O(3) (Table 3). The radii of these cations, ca. 2.17−1.32 = 0.85 Å, is sharply less than those of the In^+ ions at sites II, indicating a higher oxidation state than 1+. These radii are similar to those (0.93 and 0.91 Å) of the $In^{1.75+}$ ions found in $In_{88}-X$ and $In_{87}-X$, respectively, indicating again that these are In^{2+} or $In^{1.75+}$ (see Table 5). Those values are close to the average value, 0.95 Å, of the ionic radii of the adjacent cations in the periodic table, Cd^{2+} (0.97 Å) and Sn^{2+} (0.93 Å).[62,63] $In^{ca.2+}$ ions had been seen before in In−A,[32] In−A(S_2),[33] In−A(xInSH),[35] $In_{88}-X$, and $In_{87}-X$.[34] In^{2+} had also been seen before in some indium trihalide dimers[69,70] such as $[In_2Cl_6]^{2-}$.

These $In^{ca.2+}$ ions at In(I′) are recessed 1.01 Å into the sodalite units from the (111) planes of three O(3) oxygens (Table 4). The O(3)−In(I′)−O(3) angle, 100.1(2)°, is somewhat close to 109.47°, indicating that these $In^{ca.2+}$ ions may have near tetrahedral environments. Furthermore, In^{2+} has an odd number of electrons and is an unstable oxidation state; it might be stabilized by further coordination. The eight In^0 atoms per unit cell at site U (vide infra) complete these tetrahedra in all sodalite units (one in each sodalite unit) to give centered tetrahedral clusters of $(In^{ca.2+})_4In^0$, most likely $(In_5)^{7+}$. A stereoview of the sodalite unit is shown in Figure 6.

Finally, one In^{2+} ion per unit cell is found at another site II, at In(IIa), on a 3-fold axis opposite a S6R. It is 2.25(3) Å from the S6R oxygens at O(2) (see Table 3), confirming its oxidation number (2+) with an ionic radius of ca.. 0.93 Å = 2.25−1.32 (vide supra). This In^{2+} ion is recessed 0.83 Å into the supercage from the (111) plane of the three S6R O(2) oxygens (see Table 4). The O(2)−In(IIa)−O(2) angle is 112(2)°, nearly tetrahedral, suggesting an additional ligand in the supercage. This possible ligand could not be confirmed crystallographically because of its low occupancy, its likely small scattering power, and its virtual closeness to the In(II) position.

(d) Indium Atoms at Site U. The eight indiums per unit cell at In(U) fill the 8-fold position and make no close approaches to any framework atoms (see Tables 2 and 3). However, they are reasonably close to the $In^{ca.2+}$ ions at In(I′) in the sodalite unit, indicating that they are In atoms (In^0) bound to the $In^{ca.2+}$ cations. Furthermore, the location of the In^0 at In(U) is

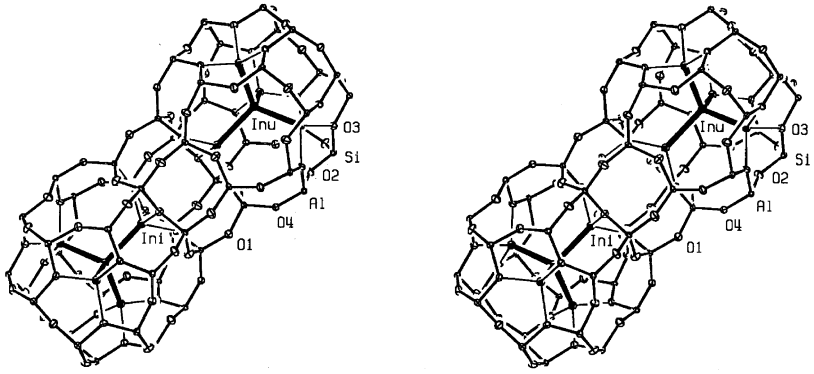

Figure 7. Stereoview of two adjacent sodalite units in $In_{66}-X$, with In_5^{n+} clusters at their centers. See the captions to Figures 5 and 6 for other details.

unambiguous, because no other chemically possible atom or ion, such as Si, Al, S, O, or N, which might have been produced and retained during the reactions between In and Tl−X and/or introduced during later exposures to air, water, or H_2S, could account for the electron density found (ca. 387 eÅ^{-3}/8 = 48 eÅ^{-3}) at this special position.

Some of the eight In^0 atoms per unit cell might have been retained from the initial reaction between In^0 and Tl−X. Others must be the product of the in-situ disproportionation of In^+, i.e., $2In^+ \rightarrow In^{2+} + In^0$, as seen in the crystal structures of the reactant $In_{87}-X$ (2.5 In^0 per unit cell) and that of its precursor $In_{88}-X$ (2.0 In^0 per unit cell).[34] Some of those 2.5 or 2.0 In^0 atoms might also have been produced by further disproportionation upon later exposure to the atmosphere or to deionized water, or both, during the preparation of the reactant $In_{87}-X$. (The In^0 and $In^{ca.2+}$ occupancies both increased, from 2.0 and 8.0 in $In_{88}-X$ to 2.5 and 10.0 in $In_{87}-X$, respectively.) Therefore, the additional 5.5 In^0 atoms and 22 $In^{ca.2+}$ ions per unit cell at In(U) and In(I′), respectively, of the product $In_{66}-X$ must have been produced during the exposure of $In_{87}-X$ to H_2S at 673 K.

The In^0 atom at In(U) is 2.683(1) Å from the $In^{ca.2+}$ cation at In(I′) (see Table 3). This is a reasonable bonding distance for $In^0-In^{ca.2+}$, considering that the sum of atomic and ionic radii of In^0 and $In^{ca.2+}$ is 2.53 (or 2.49) Å = 1.67 (or 1.63) + 0.86 Å, respectively.[71] This reasonable distance further affirms the presence of $(In^{ca.2+})_4In^0$ clusters, four $In^{ca.2+}$ ions tetrahedrally arranged in each sodalite unit with an In^0 atom at their center to give $(In_5)^{7+}$.

(e) The $(In_5)^{n+}$ Cation in the Sodalite Cavity. The In atoms at site U preferentially approach cations rather than framework oxygens because the cations have both a higher absolute charge and are smaller and therefore have more polarizing power. Some coordination of In^0 is necessary to support it in space at its position far from the zeolite framework, and In(I′) is the only "ligand" position available. Finally, In^0 should coordinate to $In^{ca.2+}$ rather than In^+ because $In^{ca.2+}$ has more polarizing power and because In^{2+} is the less stable oxidation state (an odd electron cation). All of the sodalite units in $In_{66}-X$ contain an $(In^{ca.2+})_4In^0$ cluster (see Figure 6).

Some delocalization of electron density from In^0 to the $In^{ca.2+}$ ions must occur in $(In^{ca.2+})_4In^0$, so both of these oxidation states must be considered only approximate. As discussed above, it is best to consider the charge of the $(In_5)^{n+}$ cation rather than the charge of the In "atom" at site U and the In cation at site I′. Accordingly, to complete a stable octet of electrons about the central atom, the actual charge of the $(In_5)^{n+}$ cluster is proposed to be 7+ as was done before for In−A and In−X.[34,35]

If $n = 7$ in $(In_5)^{n+}$, the sum of the cationic charges due to In species would be only 83+ per unit cell, insufficient to balance the 92− initial framework charge. To achieve charge balance, 4.5 of the 384 oxygen atoms (oxide ions) per unit cell may have been lost. The diminished In content of $In_{66}-X$ as compared to $In_{87}-X$ and the dark powder observed on the surface of the $In_{66}-X$ crystal support such a loss of framework oxygen, perhaps by one of the following reactions, both of which give a black product that would not be expected to vaporize away from the surface of the crystal at 673 K

$$O^{2-} + H_2S + In^{2+} \rightarrow InS + H_2O$$

or

$$3O^{2-} + 3H_2S + 3In^{2+} \rightarrow In_2S_3 + 3H_2O + In^0$$

The In^{2+} ions used for these reactions would have been present initially or may be viewed as a product of the disproportionation of In^+.

Alternatively, if framework oxygen is not lost as water, nine H^+ ions (from H_2S) would need to be present per unit cell, perhaps by one of the following reactions:

$$H_2S + In^{2+} \rightarrow InS + 2H^+$$

or

$$3H_2S + 3In^{2+} \rightarrow In_2S_3 + 6H^+ + In^0$$

The H^+ ions could occupy available sites near In(II), In(IIa), III, or III′. However, it would be expected that H^+ ions would react with framework oxygens at 673 K. The loss of 4.5 (out of 384) framework oxgyens per unit cell should not affect the intensity of the diffraction from $In_{66}-X$ much, especially with strongly scattering $(In_5)^{7+}$ cations in all sodalite units. However, it could readily have led to the loss of long-range Si/Al ordering, making the use of the $Fd\bar{3}$ space group inappropriate. Further work to determine experimentally the charge of the $(In_5)^{n+}$ clusters is in progress.

(f) An Array of In_5^{n+} quantum Dots. The $(In_5)^{n+}$ cluster can be considered to be an isolated quantum dot with a radius of ca. 3.5 Å (the $In^0-In^{ca.2+}$ bond length (2.68 Å) + the $In^{ca.2+}$ radius (0.85 Å)). Each $(In_5)^{n+}$ cluster is well-stabilized by 12 strong interactions with framework oxygens ($In^{ca.2+}-O(3)$ = 2.170(7) Å) in a sodalite unit (see Figure 6). Each is well-isolated from other clusters (see Figure 7). Because each sodalite unit contains an $(In_5)^{n+}$ cluster, these clusters are arranged in space like the sodalite units, in the diamond structure, filling

the three-dimensional space of the resulting $In_{66}-X$ single crystal with intercluster distances ($(In_5)^{n+}-(In_5)^{n+}$) of ca. 10.8 Å, forming a spatially ordered array of $(In_5)^{n+}$ quantum dots. This array contains ca. 300 Tera (10^{12}) ordered quantum dots in the octahedral In−X single crystal used, whose cross-section was ca. 0.15 mm.

With a technology that would enable each $(In_5)^{n+}$ cluster to be tagged electronically or magnetically, a single crystal of $In_{66}-X$ could be used as a storage medium with a capacity of the order of Teras.

Acknowledgment. N.H.H. gratefully acknowledges the support of the Central Laboratory of Kyungpook National University for the use of the X-ray diffractometer. We thank Jeong Seok Noh and Han Soo Kim for their assistance in X-ray and spectroscopic data collection, respectively. This work was supported in part by the Nano Science & Technology Center of Kyungpook National University, Korea.

Supporting Information Available: Observed and calculated structure factors squared with esds for $In_{66}-X$. This material is available free of charge via the Internet at http://pubs.acs.org.

References and Notes

(1) Ozin, G. A.; Kuperman, A.; Stein, A. *Angew. Chem., Int. Ed. Engl.* **1989**, *28*, 359−376.
(2) Barrer, R. M. *Hydrothermal Chemistry of Zeolites*; Academic Press: New York, 1972.
(3) Breck, D. W. *Zeolite Molecular Sieves*; John Wiley & Son: New York, 1974.
(4) Srdanov, V. I.; Blake, N. P.; Markgraber, D.; Metiu, H.; Stucky, G. D. *Advanced Zeolite Science and Applications, Studies in Surface Science and Catalysis*: Jansen, J. C., Stocker, M., Karge, H. G., Weitkamp, J., Eds.; Elsevier Science: Amsterdam, 1994; Vol. 85, pp 115−144.
(5) Fox, M. A.; Pettit, T. L. *Langmuir* **1989**, *5*, 1056−1061.
(6) Stucky, G. D.; MacDougall, J. E. *Science* **1990**, *247*, 669−678.
(7) Moller, K.; Bein, T.; Herron, N.; Mahler, W.; Macdougall, J. E.; Stucky, G. D. *Mol. Cryst. Liq. Cryst.* **1990**, *181*, 305−314.
(8) Uchida, H.; Ogata, T.; Yoneyama, H. *Chem. Phys. Lett.* **1990**, *173* (1), 103−106.
(9) Moran, K. L.; Harrison, W. T. A.; Kamber, I.; Gier, T. E.; Bu, X. H.; Herren, D.; Behrens, P.; Eckert, H.; Stucky, G. D. *Chem. Mater.* **1996**, *8*, 1930−1943.
(10) Wang, Y.; Herron, N. *J. Phys. Chem.* **1987**, *91*, 257−260.
(11) Kuczynski, J.; Nakamura, T.; Thomas, J. K. *J. Phys. Chem.* **1985**, *89*, 2720−2722.
(12) Stramel, R. D.; Thomas, J. K. *J. Chem. Soc., Faraday Trans. 1* **1988**, *84*, 1287−1300.
(13) Kitagawa, H.; Sendoda, Y.; Ono, Y. *J. Catal.* **1986**, *101*, 12−18.
(14) Gnep, N. S.; Doyemet, J. Y.; Seco, A. M.; Famoa, R. F.; Guisnet, M. *Appl. Catal.* **1988**, *43*, 155−166.
(15) Kanazirev, V.; Price, G. L.; Dooley, K. M. *Zeolite Chemistry and Catalysis*; Jacobs, P. A., Ed.; Elsevier: Amsterdam, 1991; pp 227−285.
(16) Kanazirev, V.; Valtchev, V.; Tarassov, M. P. *J. Chem. Soc. Chem. Commun.* **1994**, 1043−1044.
(17) Mowry, J. R.; Anderson, R. F.; Johnson, J. A. *Oil Gas J.* **1985**, 128−131.
(18) Kanazirev, V.; Price, G. L.; Dooley, K. M. *J. Chem. Soc., Chem. Commun.* **1990**, 712−713.
(19) Price, G. L.; Kanazirev, V. *J. Catal.* **1990**, *126*, 267−278.
(20) Chatterjee, M.; Bhattcharya, D.; Hayashi, H.; Ebina, T.; Onodera, Y.; Nagase, T.; Sivasanker, S.; Iwasaki, T. *Microporous Mesoporous Mater.* **1998**, *20*, 87−91.
(21) Mihalyi, R. M.; Beyer, H. K.; Mavrodinova, V.; Minchev, Ch.; Neinska, Y. *Microporous Mesoporous Mater.* **1998**, *24*, 143−151.
(22) Ogura, M.; Ohaski, T.; Kikuchi, E. *Microporous Mesoporous Mater.* **1998**, *21*, 533−540.
(23) Kanazirev, V.; Neinska, Y.; Tsoncheva, T.; Kosova, L. *Proceedings of the Ninth International Zeolite Conference*; van Ballmoos, R., Higgins, J. B., Tracy, M. M. J., Eds.; Butterworth-Heinemann: New York, 1993; pp 461−468.
(24) Heo, N. H.; Choi, H. C. Unpublished results.
(25) Alekseev, Yu. A.; Bogomolov, V. N.; Egorov, V. A.; Petranovskii, V. P.; Kholodkevich, S. V. *JETP Lett.* **1982**, *36*, 463−465.
(26) Alekseev, Yu. A.; Bogomolov, V. N.; Zhukova, T. B.; Petranovskii, V. P.; Kholodkevich, S. V. *Sov. Phys. Solid State* **1982**, *24* (8), 1384−1388.
(27) Blackwell, C. S.; Pluth, J. J.; Smith, J. V. *J. Phys. Chem.* **1985**, *89*, 4420−4423.
(28) Bogomolov, V. N.; Petranovskii, V. P. *Zeolites* **1986**, *6*, 418−419.
(29) Heo, N. H.; Seff, K. *J. Am. Chem. Soc.* **1987**, *109*, 7986−7992.
(30) Heo, N. H.; Seff, K. *Perspectives in Molecular Sieve Science*; ACS Symposium Series 368; Flank, W. H., Whyte, T. E., Jr., Eds.; American Chemical Society: Washington, DC, 1988; pp 177−193.
(31) Sun, T.; Seff, K. *J. Phys. Chem.* **1993**, *97*, 5213−5214.
(32) Heo, N. H.; Choi, H. C.; Jung, S. W.; Park, M.; Seff, K. *J. Phys. Chem. B* **1997**, *101*, 5531−5539.
(33) Heo, N. H.; Kim, S. H.; Choi, H. C.; Jung, S. W.; Seff, K. *J. Phys. Chem. B* **1998**, *102*, 17−23.
(34) Heo, N. H.; Jung, S. W.; Park, S. W.; Park, M.; Lim, W. T.; Seff, K. *J. Phys. Chem. B* **2000**, *104*, 8372−8381.
(35) Heo, N. H.; Chun, C. W.; Park, J. S.; Lim, W. T.; Park, M.; Li, S. L.; Zhou, L. P.; Seff, K. *J. Phys. Chem. B* **2002**, *106*, 4578−4587.
(36) Thiel, A. *Z. Anorg. Chem.* **1904**, *40*, 280.
(37) Ashraf, M.; Aziz-Alrahmam, A. M.; Headbridge, J. B. *J. Chem. Soc., Dalton Trans.* **1977**, 170−173.
(38) Biedermann, G.; Wallin, T. *Acta Chem. Scand.* **1960**, *14*, 594−608.
(39) Kim, Y.; Han, Y. W.; Seff, K. *Zeolites* **1997**, *18*, 325−333.
(40) Firor, R. L.; Seff, K. *J. Am. Chem. Soc.* **1977**, *99*, 4039−4044.
(41) Riley, P. E.; Seff, K.; Shoemaker, D. P. *J. Phys. Chem.* **1972**, *76*, 2593−2597.
(42) Wade, K.; Banister, A. J. *Comprehensive Inorganic Chemistry*; Bailar, J. C., Jr., Ed.; Pergamon Press: Oxford, 1973; Vol. 1, pp 997−1000.
(43) Bae, D.; Seff, K. *Microporous Mesoporous Mater.* **2001**, *42*, 299−306.
(44) Yeom, Y. H.; Jang, S. B.; Kim, Y.; Song, S. H.; Seff, K. *J. Phys. Chem. B* **1997**, *101*, 6914−6920.
(45) Jang, S. B.; Jeong, M. S.; Kim, Y.; Seff, K. *J. Phys. Chem. B* **1997**, *101*, 9041−9045.
(46) *International Tables for X-ray Crystallography*; Ibers, J. A., Hamilton, W. C., Eds.; Kynoch Press: Birmingham, England, 1974; Vol. IV, pp 61−66.
(47) Sheldrick, G. M. *SHELXL97, Program for the Refinement of Crystal Structures*; University of Gottingen: Germany, 1997.
(48) Doyle, P. A.; Turner, P. S. *Acta Crystallogr., Sect. A* **1968**, *24*, 390−397.
(49) *International Tables for X-ray Crystallography*; Ibers, J. A., Hamilton, W. C., Eds.; Kynoch Press: Birmingham, England, 1974; Vol. IV, pp 71−98.
(50) Cromer, D. T. *Acta Crystallogr.* **1965**, *18*, 17−23.
(51) *International Tables for X-ray Crystallography*; Ibers, J. A., Hamilton, W. C., Eds.; Kynoch Press: Birmingham, England, 1974; Vol. IV, pp 149−150.
(52) *Handbook of Chemistry and Physics*, 74th ed.; Chemical Rubber Co.; Cleveland, OH, 1993; pp 10−258.
(53) *Handbook of X-ray Photoelectron Spectroscopy*; Perkin-Elmer Co.: Eden Prairie, MN, 1992; pp 124−125.
(54) Stocker, M. *Microporous Mater.* **1996**, *6*, 235−257.
(55) Olson, D. H. *Zeolites* **1995**, *15*, 439−443.
(56) Sun, T.; Seff, K. *Chem. Rev.* **1994**, *94*, 859.
(57) Loewenstein, W. *Am. Mineral.* **1954**, *39*, 92−96.
(58) Zhu, L.; Seff, K. *J. Phys. Chem. B* **1999**, *103*, 9512−9518.
(59) Bae, D.; Zhen, S.; Seff, K. *J. Phys. Chem. B* **1999**, *103*, 5631−5636.
(60) Zhu, L.; Seff, K.; Olson, D. H.; Cohen, B. J.; Von Dreele, R. B. *J. Phys. Chem. B* **1999**, *103*, 10365−10372.
(61) Bae, D.; Seff, K. *Microporous Mesoporous Mater.* **1999**, *33*, 265−280.
(62) Shannon, R. D.; Prewitt, C. T. *Acta Crystallogr., Sect. B* **1969**, *25*, 925−946.
(63) *Handbook of Chemistry and Physics*, 64th ed.; Chemical Rubber Co.: Cleveland, OH, 1983; p F-187.
(64) Brode, H. *Ann. Phys.* **1940**, *37*, 344.
(65) Barrett, A. H.; Mandel, M. *Phys. Rev.* **1955**, *99*, 666.
(66) Barrow, R. F.; Glaser, D. V.; Zeeman, P. B. *Proc. Phys. Soc., London, Sect. A* **1955**, *68*, 962−968.
(67) Kim, Y.; Seff, K. *J. Phys. Chem.* **1978**, *82*, 1307−1311.
(68) Fraga, S.; Saxeua, K. M. S.; Karwowski, J. *Handbook of Atomic Data*; Elsevier Scientific: Amsterdam, 1976; p 465.
(69) Stevenson, D. P.; Schomaker, V. *J. Am. Chem. Soc.* **1942**, *64*, 2514−2514.
(70) Cotton, F. A.; Wilkinson, G. *Advanced Inorganic Chemistry*, 5th ed.; John Wiley & Sons: New York, 1988; pp 209−233.
(71) Tyzack, G.; Raynor, G. V. *Trans. Faraday Soc.* **1954**, *50*, 675−680.